Composites Science and Technology 239 (2023) 110052

Contents lists available at ScienceDirect

Composites Science and Technology

journal homepage: www.elsevier.com/locate/compscitech

Rapid-actuating high-T_g shape memory polyimide composites with synergistic "micro-nano" thermal conduction networks

Xiaofei Wang [a], Yang He [a], Xinli Xiao [b], Jinsong Leng [a,*]

[a] Center for Composite Materials and Structures, Harbin Institute of Technology, Harbin, 150080, PR China
[b] MIIT Key Laboratory of Critical Materials Technology for New Energy Conversion and Storage, School of Chemistry and Chemical Engineering, Harbin Institute of Technology, Harbin, 150001, PR China

ARTICLE INFO

Handling Editor: W. Yang

Keywords:
Polymer-matrix composites
Smart material
High-temperature properties
Shape memory behavior
Heat treatment

ABSTRACT

Shape memory polyimide (SMPI) is one of the most promising intelligent materials and has a high potential for deformable flexible electrodes, intelligent thermal management devices, and high temperature active deployable structures, etc. In this paper, silane-modified AlN nanoparticles (M-AlN) are composited with SMPI matrix resin to prepare fast-response high-T_g shape memory composites. Besides, nano-sized AlN and micron-sized Al_2O_3 are used to construct "micro-nano" synergistic thermal conduction networks, in which the AlN acted as the "thermal conduction island", and the Al_2O_3 acted as the "thermal conduction bridge". The results show that the in-plane thermal conductivity of Al_2O_3/M-AlN/M-SMPI-2 is 5.99 W $m^{-1}K^{-1}$, compared with SMPI, its thermal conductivity increases by 91%. In addition, the shape transition temperature of Al_2O_3/M-AlN/M-SMPI-2 was higher than that of pure SMPI, which was at 426 °C, and the thermal response shape recovery speed is also greatly improved by 433%, which can be used in rapid-actuating and high temperature active deformation structure.

1. Introduction

Shape memory polymer (SMP) refers to an intelligent polymer which could program an initial shape to a new temporary shape and restore its original status under the external stimulations, such as heat, electricity, light, magnetism, chemical solvents, or water, etc. [1–8], which has broad application prospects in intelligent actuators, soft robots, flexible electronics, biomedical fields, and aerospace fields [9–14]. SMPs consist of shape memory polyurethane [15], shape memory EVA [16], shape memory PCL [17], and shape memory PLA [18], etc. Certain SMPs can withstand harsh environments, including shape memory polyimide (SMPI) [19], shape memory epoxy resin [20], shape memory cyanate resin [21], and shape memory bismaleimide resin [22], etc. However, there are few SMPs with a transition temperature over 400 °C, which limits the applications in the high temperature environment.

Polyimide (PI) refers to a class of polymers containing imide rings (–CO–N–CO–) on the main chains, which is one of the organic polymer materials with the best comprehensive properties [23,24]. Yu et al. [25] produced a light-colored SMPI with a shape memory transition temperature (T_{trans}) of 320–380 °C, which was synthesized by grafting 0–8 wt% caged polysilsesquioxane onto the SMPI matrix. Besides, the T_{trans} of most SMPIs remain below 400 °C, while the T_{trans} of our SMPI composite has exceeded 425 °C, which is an advance news. Afterall, the T_{trans} of pure SMPI and its composite at present are 416 °C and 399 °C, respectively [26].

In order to improve the thermal conductive of materials, some particles are often doped in the matrix resin, such as graphene, carbon nanotubes, gold nanoparticles, silver nanowires, Al_2O_3, MgO, BN, and AlN, etc. [27–31]. Zhou et al. reported that the thermal conductivity of the 5 wt% AlN/PP composites reached about 0.17 W $m^{-1}K^{-1}$ and had an enhancement of 13.3% compared with pure PP materials [32]. Al_2O_3/epoxy composite was prepared by Wu et al., and when the content of Al_2O_3 was 40 wt%, the thermal conductivity rose to 1.26 W $m^{-1}K^{-1}$, resulting in 500% higher than that of epoxy resin matrix [33]. The thermal conduction property of the composite was poor when a kind of particles was simply added, unless the amount was large, thus, researchers have developed binary fillers reinforcement. Z. Barani et al. [34] fabricated an epoxy-based binary composites, of which the thermal conductivity was 13.5 ± 1.6 W $m^{-1}K^{-1}$ with 40 wt% graphene and 35 wt% Cu nanoparticles. Wang et al. [35] reported thermally conductive synergistic enhancement polyimide composite films, among them, the maximum thermal conductivity of 11.203 W $m^{-1}K^{-1}$ was achieved at fillers loading of 1 wt% graphene oxide and 20 wt % BN, while the maximum storage modulus was lower than 3 GPa. Although there are

* Corresponding author.
E-mail address: lengjs@hit.edu.cn (J. Leng).

https://doi.org/10.1016/j.compscitech.2023.110052
Received 14 January 2023; Received in revised form 21 March 2023; Accepted 24 April 2023
Available online 25 April 2023

some researches on binary fillers to enhance thermal conductivity, few have applied to SMP to improve response speed. At present, it can be just found that D.I. Arun et al. [36] doped 5 wt% carbon black and 0.25 wt% multi-walled carbon nanotubes into shape memory polyurethane to improve the response speed to 41 s. SMPI has a very high transition temperature and a very long recovery time, so, how to speed up the response speed, adapt to extremely harsh environment, and maintain high comprehensive performances are urgent issues to be solved.

In this paper, the silane-modified AlN nanoparticles (M-AlN) was adopted to prepare high shape transition temperature SMPI composites with good compatibility and high thermal conductivity. Also, the synergistic "micro-nano" networks were constructed, in which the nano-sized AlN acted as the "thermal conduction island", and the micro-sized Al_2O_3 acted as the "thermal conduction bridge", thus greatly improving the interconnection property of the thermal conduction networks, and enabling SMPI recover its original shape more quickly. The in-plane thermal conductivity of Al_2O_3/M-AlN/M-SMPI-2 was 5.99 W $m^{-1}K^{-1}$, compared with pure SMPI, the thermal conductivity increased by 91%, and the thermal response shape recovery speed was also greatly improved by 433%. The SMPI composites have application prospects in the fields of deformed flexible electrodes, aerospace deployable structures and high-temperature active deformation devices.

2. Experiment section

2.1. Raw materials and reagents

5-Amino-2-(4-aminophenyl) benzimidazole (DAPBI), 3,3′,4,4′-biphenyltetracarboxylic dianhydride (BPDA), silane coupling agent KH-550, AlN nanoparticles (300–500 nm), and Al_2O_3 microparticles (5–6 μm) were all from Shanghai Aladdin Reagent Co., Ltd. Ethanol and dimethyl sulfoxide (DMSO) came from Tianjin Fengchuan Chemical Reagent Technology Co., Ltd. Deionized water came from Harbin Institute of Technology.

2.2. Preparation of rapid-actuating high-T_g SMPI composites

2.2.1. Surface modification of AlN nanoparticles (M-AlN)

According to the literature [37], we modified the surface of the AlN nanoparticles. The AlN nanoparticles were dispersed in ethanol/water (95/5) under the action of ultrasound field, then, the silane coupling agent KH-550/ethanol solution was dropped into the AlN/ethanol/-water mixture and was reacted at 70 °C for 2 h (The KH-550 accounted for 5 wt% of AlN particles). The mixed solution was centrifuged at 4000 rpm/min for 5 min, and washed for 5 times by absolute ethanol, then, they were put into an oven at 40 °C for 48 h, and the surface-modified AlN nanoparticles were produced, named M-AlN.

2.2.2. Preparation of M-AlN/SMPI composites by in situ polymerization (M-AlN/M-SMPI)

(I) A certain amount of M-AlN was put into DMSO solvent and then ultrasound field for 30 min; after that, DAPBI was added to the system to dissolve fully, also, BPDA was put into the system in 5 times (the molar ratio of DAPBI and BPDA was 1:1). The stirring speed of the mixture was 250 r/min for 120 h at room temperature to gain polyamic acid (PAA) solution. The solid content of PAA solution was 17 wt%, and the contents of M-AlN were 2 wt%, 4 wt%, 6 wt%, 8 wt%, and 10 wt%, respectively.

(II) The PAA solution was poured into a glass plate and placed in an oven to conduct thermal imidization reaction, and rapid-actuating high-T_g SMPI composites (M-AlN/M-SMPI) were fabricated. The heating steps were that 50 °C for 5 h, 80 °C for 5 h, 120 °C for 2 h, 160 °C for 2 h, 200 °C for 2 h, 250 °C for 2 h, and 300 °C for 2 h. The SMPI composites were named as M-AlN/M-SMPI-2, M-AlN/M-SMPI-4, M-AlN/M-SMPI-6, M-AlN/M-SMPI-8, and M-AlN/M-SMPI-10, successively. The synthesis route and preparation process were shown in Fig. 1.

2.2.3. Construction of micro-nano multi-levels thermal conduction composites (Al_2O_3/M-AlN/M-SMPI)

(I) A certain amount of M-AlN and Al_2O_3 microparticles were added to DMSO solvent and ultrasound for 30 min; then, the following step was similar to section 2.2.2 (I). The contents of M-AlN was 6 wt%, and Al_2O_3 microparticles was 1 wt%, 2 wt%, 3 wt%, 4 wt%, and 5 wt%, respectively.

(II) This step was similar to section 2.2.2 (II). The micro-nano multi-levels thermal conduction SMPI composites were named as Al_2O_3/M-AlN/M-SMPI-1, Al_2O_3/M-AlN/M-SMPI-2, Al_2O_3/M-AlN/M-SMPI-3, Al_2O_3/M-AlN/M-SMPI-4, and Al_2O_3/M-AlN/M-SMPI-5, successively. The synthesis route and preparation process were shown in Fig. 1.

2.3. Characterization

AVATAR360 FTIR spectrometer was utilized to test the molecular structure of SMPI composite films. WAXD was used to characterize the crystallinity of pure SMPI and SMPI composites. The scanning angle was 5–80 °, and the scanning speed was 8 °/min. DMA Q800 (TA Corporation, USA) can characterize the dynamic mechanical properties of SMPI composites, of which the test conditions were that the temperature range was 25–560 °C, the temperature rise/fall rate was 5 °C/min, 1 Hz frequency, 0.2% amplitude. TGA/DSC1 synchronous thermal analyzer (METTLER-TOLEDO Corporation, Switzerland) was used to illustrate the thermal stability of SMPI composites. Test conditions were as follows: the weight of 5–10 mg, the temperature range of 25–800 °C, N_2 environment. The particles dispersion performances were characterized by SU5000 scanning electron microscope (SEM, JEOL Corporation, Japan). The out-of-plane and in-plane thermal conductivity were measured by a laser thermal conductivity meter (NETZSCH LFA 467, Germany). Zwick tensile testing machine was used to test the tensile properties of SMPI composites. The size was prepared based on GB/T528-2009. Thermal-actuated shape memory properties were as follows: Firstly, the sample was risen to T_g + 30 °C, then, external stress was applied to stretch the sample from ε_0 to $\varepsilon_0 + \Delta L$ strain. After that, the sample was fallen to 250 °C, and the stress was removed, at this time, the strain was reduced to $\varepsilon_0 + \Delta L'$. At last, the sample was reheated to T_g + 30 °C to gain the recovery strain ε_{rec}.

The equations of shape fixation ratio (R_f) and shape recovery ratio (R_r) were as follows:

$$R_f = \frac{\varepsilon_0 + \Delta L'}{\varepsilon_0 + \Delta L} \times 100\% \quad (1)$$

$$R_r = \frac{\varepsilon_{rec}}{\varepsilon_0 + \Delta L'} \times 100\% \quad (2)$$

Where, $\varepsilon_0 + \Delta L$ stood for the highest strain under external stress, $\varepsilon_0 + \Delta L'$ stood for the fixed strain after the external stress removed, and ε_{rec} stood for the shape recovered strain.

3. Results and discussion

3.1. FTIR analysis of the M-AlN/M-SMPI composites

The images of M-AlN/M-SMPI composite films were shown in Supporting information, Scheme 1. When the content of M-AlN nanoparticles was 2 wt%, 4 wt%, and 6 wt%, M-AlN/M-SMPI can form completely films, and as the content of M-AlN increased to 8 wt% and 10 wt%, the films were uneven and had partly cracking. The molecular structure was characterized by FTIR. The infrared spectrum of M-AlN/

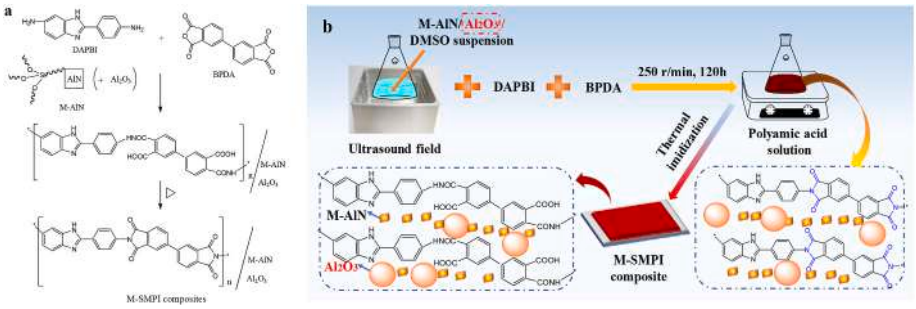

Fig. 1. (a, b) The synthesis route and preparation process of M-SMPI composites.

M-SMPI were shown in Fig. 2a, among them, the Si–O stretching vibration peak of KH550 appeared near 1079 cm^{-1}, indicating that the silane coupling agent was coated on the surface of M-AlN nanoparticles successfully. In addition, the 1355-1362 cm^{-1} in each M-AlN/M-SMPI spectrum were the characteristic absorption peaks of C–N bonds, and 1702-1709 cm^{-1} were the symmetrical stretching vibration peaks of the C═O bond, and with continuous increase of M-AlN, the two peaks positions were both shifted to the higher wavelength. This was because the strong electric absorption group $–NH_2$ in KH550 and the imine group in the M-SMPI matrix had an inductive effect, which made the interface combination performance between organic matrix and inorganic particles better. Besides, WAXD was used to characterize the influence of M-AlN on the molecular crystallinity of M-SMPI matrix, seen Supporting information, Scheme 2. With the content of the M-AlN nanoparticles increasing, the *2θ* diffraction peak intensity of the composites strengthened continuously, indicating that the crystallinity of the system increased.

3.2. The physical properties and thermal conductivity of the M-AlN/M-SMPI

From Fig. 3a, it exhibited that the storage modulus of M-AlN/M-SMPI composite was reduced constantly when the temperature was from 25 °C to 430 °C. There was a wide step between 350 °C and 430 °C, which was the glass transition temperature (T_g) area, i.e. T_{trans} area. In addition, M-AlN/M-SMPI-10 was broken during the test process, which could not be continued testing after 250 °C. On Fig. 3b, the M-AlN/M-SMPI composites had sharp peaks between 350 and 450 °C, and the temperature at the highest position was the T_g. So, the T_g/T_{trans} of the M-AlN/M-SMPI-2, -4, -6, and -8 were 413 °C, 410 °C, 418 °C, and 417 °C,

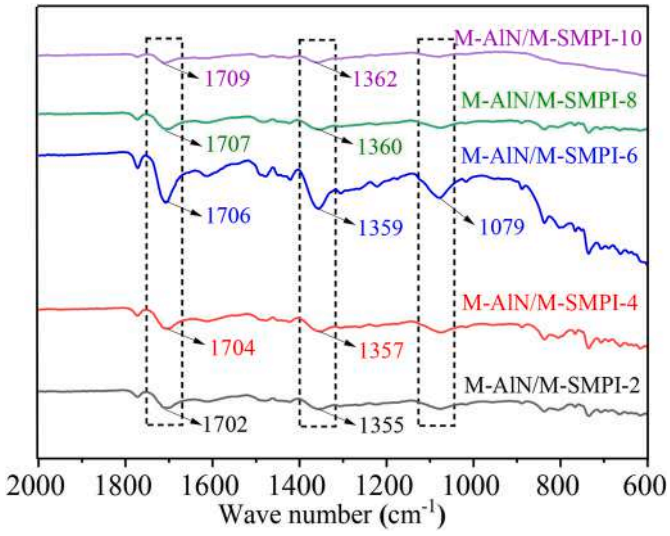

Fig. 2. FTIR spectrum of M-AlN/M-SMPI composites.

successively. However, the T_g of the pure M-SMPI film was 416 °C (The curve was shown in Supporting Information, Scheme 3), therefore, the thermal conductive particles M-AlN had little effect on the T_g of the SMPI composite materials. Besides, the thermal stability of the M-AlN/M-SMPI composites was characterized by TGA test, seen Supporting Information, Scheme 4 and Table 1. Even if the temperature reached 800 °C, the composites still possessed over 50% residue, which illustrated that the materials had good thermal stability.

The mechanical properties of M-AlN/M-SMPI composites were shown in Fig. 3c. As the M-AlN nanoparticles increasing, the tensile strength first increased and then declined, while the elongation at break decreased continuously. Because the surface of M-AlN contained silane coupling agent KH550, which can increase the compatibility between nanoparticles and the matrix. However, as the continuous increasing of nanoparticles, on the one hand, the fillers destroyed the structure regularity of M-SMPI molecular chain segments; on the other hand, M-AlN was agglomerated in the SMPI matrix, resulting in the defects and voids, and forming the stress concentration points, thus, the tensile strength and the elongation at break felled.

Furthermore, the dispersion of M-AlN nanoparticles in the M-SMPI matrix was observed by SEM, as shown in Scheme 5. It can be seen that the M-AlN nanoparticles can be uniformly dispersed in the matrix, and the average size was about 400–500 nm, which was mainly attributed to the surface modification of the nanoparticles with the silane coupling agent. The KH550 had alkoxy groups with a relatively slow hydrolysis rate and positively charged polar amino groups. One end of the hydrolyzable alkoxy groups reacted with the inorganic AlN nanoparticles, and the surface of the AlN nanoparticles formed Al–O–Si covalent bonds, so that the surface of inorganic particles obtained long-chain macromolecules, which formed steric hindrance effect to prevent the agglomeration between inorganic particles; the other end of the organic amino group interacted with the M-SMPI matrix to form hydrogen bonds. The KH550 can be used as a binder for the two-phase interfaces, which improved the interfacial bonding force between the nanoparticles and the matrix resin, and dispersed the inorganic particles with high surface energy to obtain a well-dispersed M-AlN/M-SMPI system [38].

Fig. 3d was the in-plane and out-of-plane thermal conductivity (TC) of the M-AlN/M-SMPI composite films. With the amount of the M-AlN increasing, the TC of M-AlN/SMPI composites continued increasing. Compared with M-SMPI matrix, the in-plane and out-of-plane TC of M-AlN/M-SMPI-10 increased by 97% and 62%, respectively, and M-AlN/M-SMPI-6 increased by 64% and 38%, respectively. This was mainly because as the nanoparticles increasing, they overlapped with each other and formed continuous thermal conduction networks, which greatly reduced the in-plane thermal resistance and increased the thermal conductivity. Additionally, the in-plane and out-of-plane TC differed by an order of magnitude. The reason was that the M-AlN/M-SMPI had a high anisotropy and the phonon transport was easier in the horizontal direction than in the vertical direction (The schematic diagram of surface thermal conduction of M-AlN/M-SMPI composites was shown in Supporting Information, Scheme 6.). When the M-AlN was added over 6 wt%, the increasing tendency of the thermal conductivity

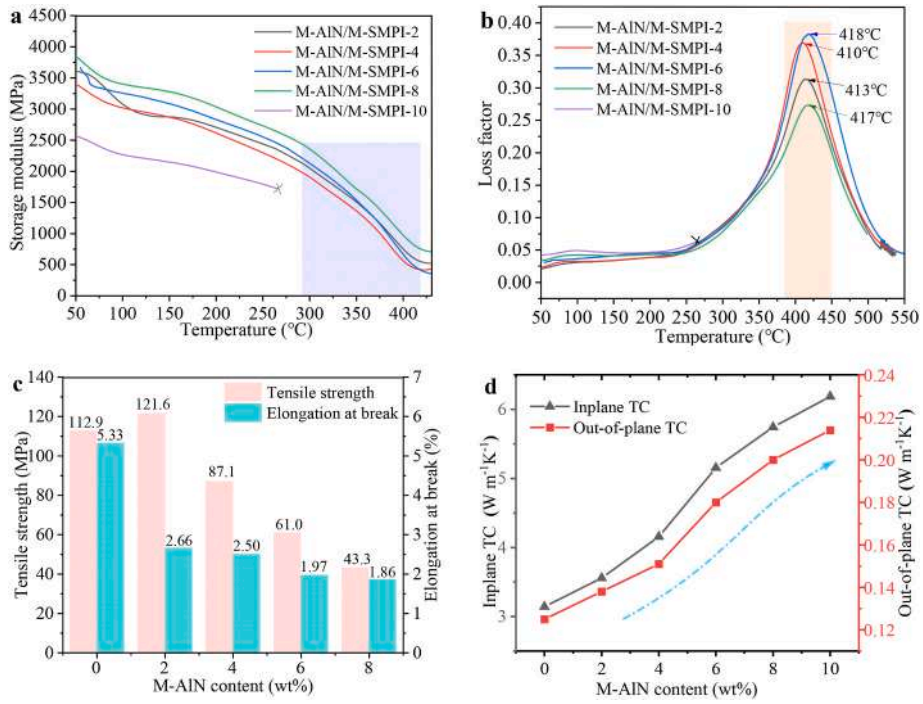

Fig. 3. (a, b) The storage modulus curves and the loss factor curves of M-AlN/M-SMPI, (c) the mechanical properties of M-AlN/M-SMPI, (d) the thermal conductivity of M-AlN/M-SMPI.

slowed down. Due to the agglomeration of the M-AlN nanoparticles in the SMPI matrix, there was a large number of defects and voids, which formed the "thermal conduction isolated island", and the heat flow cannot be well transferred, resulting in the thermal conductivity increasing slowly. Thus, it was necessary to establish "thermal conduction bridge" to enhance the thermal conduction performance.

From the above DMA, TG and thermal conductivity results, it can be seen that the performance of the M-AlN/M-SMPI-6 was relatively good, therefore, 6 wt% M-AlN nanoparticles and Al_2O_3 microparticles were used to construct micro-nano multi-level thermal conductive composites. As a result, the Al_2O_3/M-AlN/M-SMPI-1, -2, and -3 composite films was complete, while the Al_2O_3/M-AlN/M-SMPI-4, -5 films had some

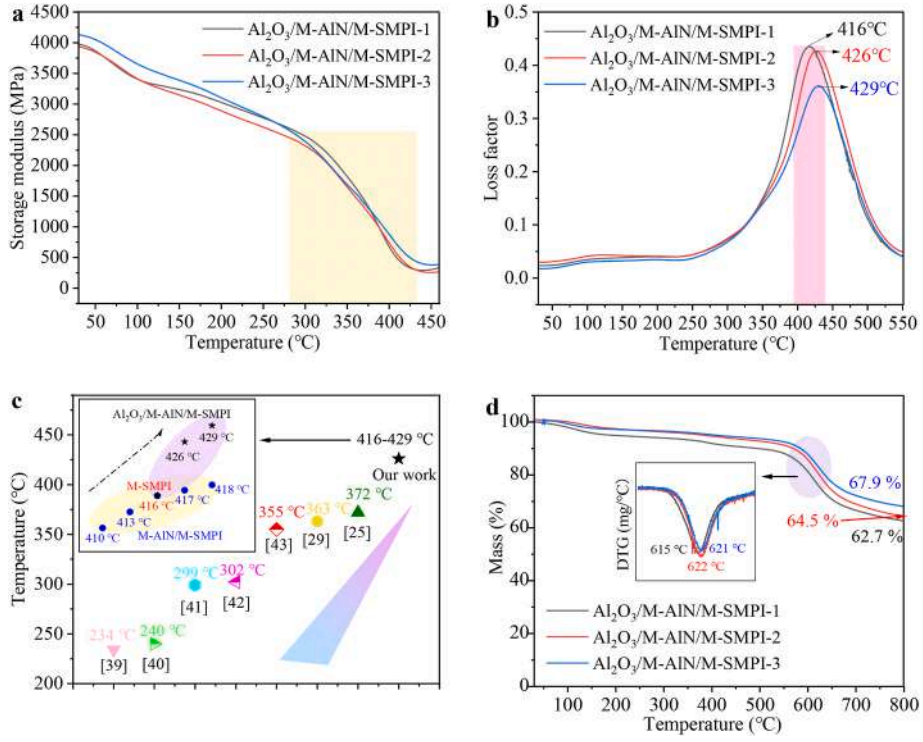

Fig. 4. (a, b) The storage modulus curves and the loss factor curves of Al_2O_3/M-AlN/M-SMPI composites, (c) comparison of transition temperature with other literatures, (d) the TGA curves of Al_2O_3/M-AlN/M-SMPI composites.

cracks. We studied the properties of the "micro-nano" thermally conductive composite films to provide a reference for the practical application of the material.

3.3. Thermomechanical properties of the Al_2O_3/M-AlN/M-SMPI

Fig. 4a showed that the storage modulus of the Al_2O_3/M-AlN/M-SMPI-1, -2, and -3 composites were 3987 MPa, 3935 MPa, and 4127 MPa, successively, which was higher than that of reference [35]. As the temperature increasing, the storage modulus was decreased continuously, and there was a wide step between 375 and 450 °C. On Fig. 4b, the Al_2O_3/M-AlN/M-SMPI composites had sharp peaks between 375 and 450 °C, and the highest position was at 416–429 °C. The T_g/T_{trans} of the Al_2O_3/M-AlN/M-SMPI-1, -2, and -3 were 416 °C, 426 °C, and 429 °C, successively, thus, the T_{trans} of the composites kept rising with the increase of the Al_2O_3 microparticles. This was because the rigidity of the molecular chain segments of the composite was enhanced, and the storage modulus at 30 °C also proved the rationality of the phenomenon. In the continuous heating process, the molecular chain segment motion was hindered, and the movement ability was also weakened, so that higher temperature was required to drive the molecular chains motion. Besides, the T_g/T_{trans} of the Al_2O_3/M-AlN/M-SMPI composite was compared with other reports [25,29,39–43], as shown in Fig. 4c. It illustrated that the transition temperature of the Al_2O_3/M-AlN/M-SMPI composite was improved compared with pure M-SMPI and other SMPIs.

The thermal stability of the Al_2O_3/M-AlN/M-SMPI composite was characterized by TGA test. Fig. 4d and Scheme 7 were the TG and DTG curves of the Al_2O_3/M-AlN/M-SMPI composites, respectively. When the temperature was below 550 °C, the TG curves decreased very slowly, indicating that the weight loss of the composites were very small. The range of the maximum decomposition rate temperature were between 615 °C and 622 °C in the DTG curves. Even if the temperature reached 800 °C, the materials still held over 50% residual quantity. Among them, the residual quantity of Al_2O_3/M-AlN/M-SMPI-1, -2, and -3 were 62.7%, 64.5%, and 67.9%, successively. The Al_2O_3 was inorganic particles, and these inorganic substances cannot be decomposed at 800 °C, therefore, the more the filler particles increased, the more the residual amount had.

Additionally, we tested the mechanical properties of the Al_2O_3/M-AlN/M-SMPI composites in Scheme 8. As the content of Al_2O_3 microparticles increasing, the tensile strength of the Al_2O_3/M-AlN/M-SMPI first increased and then decreased. Because the micro-sized Al_2O_3 filled the voids of the matrix generated by the M-AlN particles, and reduced the stress concentration points. However, as the particles continuous increasing, on one hand, the two particles destroyed the structural regularity of the molecular chain segments of the polyimide matrix; on the other hand, the two particles agglomerated in the SMPI matrix, resulting in more defects and stress concentration points, so the tensile strength decreased seriously.

3.4. Micromorphology and thermal conductivity of the Al_2O_3/M-AlN/M-SMPI

The dispersion of Al_2O_3 microparticles and M-AlN nanoparticles in the M-SMPI matrix was observed by SEM, as shown in Fig. 5a, where A, B, and C were Al_2O_3/M-AlN/M-SMPI-1, -2, and -3 dispersion images, respectively, and the particles in the purple circles were M-AlN nanoparticles with a size of 300–500 nm, and the particles in the yellow circles were Al_2O_3 microparticles with the size of 5–6 μm. It can be seen from the figure that the nano-scale M-AlN was distributed around the micron-scale Al_2O_3. Compared with Scheme 5, the vacant positions around the M-AlN were filled with Al_2O_3 particles, thus, the Al_2O_3 can be used as "bridges" between the M-AlN nanoparticles to form overall thermal conduction networks and had thermal conduction synergistic effects, which improved the TC value and shortened the response time of the SMPI composites.

Fig. 5b was the in-plane and out-of-plane thermal conductivity of the Al_2O_3/M-AlN/M-SMPI composite films. With the continuous increase of micron-sized Al_2O_3, the TC of the Al_2O_3/M-AlN/M-SMPI composite films continued rising. Compared with pure M-SMPI, the in-plane and out-of-plane TC of Al_2O_3/M-AlN/M-SMPI-2 increased by 91% and 75%, respectively, and Al_2O_3/M-AlN/M-SMPI-3 increased by 108% and 91%, respectively. And when the content of Al_2O_3 was 2 wt% and 3 wt%, the thermal conductivity exceeded that of M-AlN/M-SMPI-8 and M-AlN/M-SMPI-10, respectively, indicating that the methods of mixed multi-sized particles was effective in improving thermal conduction property. The schematic diagram of surface thermal conduction of Al_2O_3/M-AlN/M-SMPI composites was shown in Fig. 5c. The two kinds of particles formed effective thermal conduction paths [44], among them, the nano-sized AlN acted as the "thermal conduction island", and the micron-sized Al_2O_3 acted as the "thermal conduction bridge" to make the M-AlN nanoparticles fully contact, reducing the thermal resistance between the interfaces of the polyimide and particles [45].

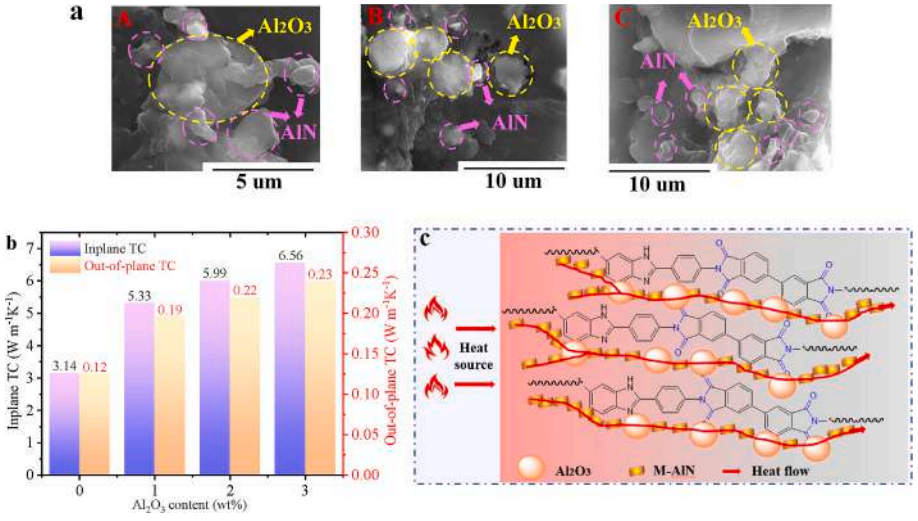

Fig. 5. (a) The SEM images of Al_2O_3/M-AlN/M-SMPI composites, (b) the thermal conductivity of Al_2O_3/M-AlN/M-SMPI, (c) the schematic diagram of surface thermal conduction of Al_2O_3/M-AlN/M-SMPI.

3.5. Shape memory properties of the SMPI composites

We used M-AlN/M-SMPI-6 to characterize the shape memory properties of the SMPI composites. Fig. 6a showed the "U" shape (i.e. bending 180°) recovered the original shape completely under heating field actuation for 45 s (Supporting information, video 1), which was 115 s shorter than that of pure M-SMPI film. Specifically, M-AlN/M-SMPI-6 was put in the 448 °C thermal field, also, the sample was shaped into a "U" shape under the external force. After that, at room temperature, the external force was removed and the sample can fix the "U" temporary shape. When the temporary shape was put into 448 °C thermal field again, it can return to the original shape completely after 45 s. Compared with pure M-SMPI (Shape recovery process was shown in Supporting Information, Scheme 9), the thermal response speed of M-AlN/M-SMPI-6 was improved by 256%, therefore, the response speed can be accelerated by adding thermal conduction particles. Similarly, we also tested the "U" shape recovery of Al_2O_3/M-AlN/M-SMPI-2 (Supporting information, video 2.), as shown in Fig. 6b, and found that the recovery time was shorter, at 30 s, of which the thermal response speed was 433% higher than that of pure M-SMPI, so the "micro-nano" binary particles were used to construct synergistic thermal conduction networks to accelerate the response speed and shorten the shape recovery time. Fig. 6c was the corrugated shape recovery process of Al_2O_3/M-AlN/M-SMPI-2, and after heating for 25 s, the corrugated shape can return to the straight status (Supporting information, video 3.). Therefore, the SMPI composites we prepared had high potential applications for smart flexible electronic devices and high-temperature active deformation.

Supplementary video related to this article can be found at https://doi.org/10.1016/j.compscitech.2023.110052

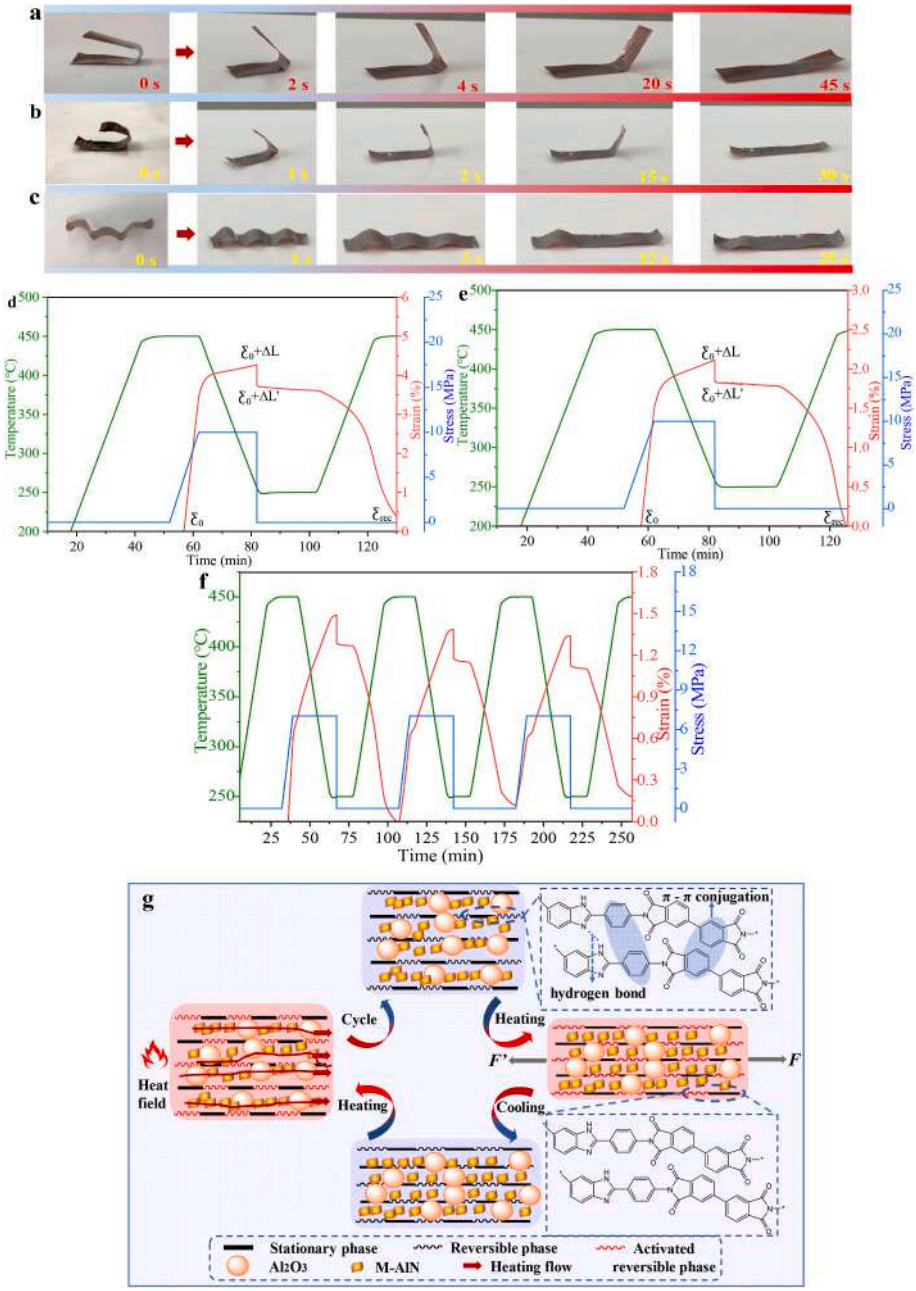

Fig. 6. (a, b) Images of the "U" shape memory process of M-AlN/M-SMPI-6 and Al_2O_3/M-AlN/M-SMPI-2, respectively, (c) images of the corrugated shape memory process of Al_2O_3/M-AlN/M-SMPI-2, (d, e) the shape memory cycles of M-AlN/M-SMPI-6 and Al_2O_3/M-AlN/M-SMPI-2 by DMA test, respectively, (f) the shape memory curves of the Al_2O_3/M-AlN/M-SMPI-2 with three cycles, (g) the shape memory mechanism of M-SMPI composites.

Fig. 6d and e were the shape memory cycle curves of M-AlN/M-SMPI-6 and Al_2O_3/M-AlN/M-SMPI-2, respectively, and both of them showed good shape memory performance. Specifically, in Fig. 6d, the shape fixation ratio and recovery ratio of the M-AlN/M-SMPI-6 were 88% and 89%, respectively. And in Fig. 6e, the shape fixation ratio of Al_2O_3/M-AlN/M-SMPI-2 was 87%, and the shape recovery ratio was 100% completely, while the shape fixation ratio and shape recovery ratio of the M-SMPI were 84.5% and 96.0%, respectively (Supporting information, Scheme 10), illustrating that the "micro-nano" thermal conductive structure was conducive to the rapid response and shape memory properties. In addition, Fig. 6f showed the shape memory curves of the Al_2O_3/M-AlN/M-SMPI-2 with three cycles, and the shape memory data was shown in Supporting Information, Table 2, which illustrated that the SMPI composites had good shape memory performances and cyclic stabilities.

The shape memory mechanism and rapid recovery mechanism of M-AlN/M-SMPI and Al_2O_3/M-AlN/M-SMPI composites are as follows. To achieve shape memory performance, the polymer matrix molecular chain structure needs a reversible phase and a stationary phase. M-AlN/M-SMPI and Al_2O_3/M-AlN/M-SMPI composites have obvious glass transition, which can be used as the reversible phase. And the stationary phase comes from macromolecular chains interaction, including chains entanglement, hydrogen bonds, and π-π conjugation effects. As shown in Fig. 6g, when the temperature is lower than the T_g of the smart composites, the molecular motion energy is low, and the chain segment motion is in a "frozen" status. When the temperature reaches the T_g of the composites, the free volume of the SMPI molecular chain increases, and the chain segment motion begins to "thaw" and inters a high elastic status. Also, under the action of external force, the composite produces a large strain. When the temperature drops below the T_g, the chain segment is "frozen" again, and a temporary shape is fixed, meanwhile, the elastic strain energy stored in the composite is not released. When heated over T_g again, since the chain segment gains enough energy and free volume, the molecular chain starts to move violently, and the elastic strain energy is gradually released, which promotes the smart composite to return from the temporary state to the original state. During the heating process, the M-AlN reduces the interface phonon scattering and lowers the interfacial thermal resistance, thereby enhancing the thermal conductivity of the M-AlN/M-SMPI composite, and the shape recovery speed is faster than that of pure M-SMPI. For the Al_2O_3/M-AlN/M-SMPI composite, the nano-sized M-AlN particles and the micro-sized Al_2O_3 form excellent thermal conduction networks, which greatly improves the response speed of the SMPI composite.

4. Conclusions

In this paper, silane-modified nanoparticles M-AlN were introduced to the M-SMPI matrix resin, and SMPI composite was prepared with good compatibility, high thermal conductivity, and high T_g. The in-plane thermal conductivity of M-AlN/M-SMPI-6 was 5.16 W $m^{-1}K^{-1}$, which was 64% higher than that of pure M-SMPI. Based on the synergistic thermal conduction effect between nano-sized M-AlN and micro-sized Al_2O_3 particles, the multi-level thermal conductive networks were constructed, and the in-plane thermal conductivity of the Al_2O_3/M-AlN/M-SMPI-2 composite was 5.99 W $m^{-1}K^{-1}$, which was 91% higher than that of pure M-SMPI. Also, the shape response speed was improved by 433%, and the shape fixation ratio and shape recovery ratio were 87% and 100%, respectively. Thus, the smart composites have broad application prospects in the fields of deformable flexible electrodes, intelligent thermal management devices, and deployable structures.

CRediT authorship contribution statement

Xiaofei Wang – Investigation, Methodology, Data curation, Visualization, Writing-original draft, Writing - review & editing. **Yang He** – Investigation, Methodology, Validation, Resources, Project administration, Writing - review & editing. **Xinli Xiao** – Investigation, Methodology, Validation, Writing - review & editing. **Jinsong Leng** – Conceptualization, Supervision, Project administration, Funding acquisition, Writing-reviewing & editing.

Declaration of competing interest

The authors declare that they have no known competing financial interests or personal relationships that could have appeared to influence the work reported in this paper.

Data availability

Data will be made available on request.

Acknowledgements

This work is supported by the National Key R&D Program of China (2022YFB3805700).

Appendix A. Supplementary data

Supplementary data to this article can be found online at https://doi.org/10.1016/j.compscitech.2023.110052.

References

[1] F. Zhao, X.Y. Zheng, S.C. Zhou, B. Zhou, S.F. Xue, Q. Zhang, Constitutive model for epoxy shape memory polymer with regulable phase transition temperature, Int. J. Smart Nano Mater. 12 (1) (2021) 72–87, https://doi.org/10.1080/19475411.2021.1876176.

[2] M. Herath, J. Epaarachchi, M. Islam, L. Fang, J.S. Leng, Light activated shape memory polymers and composites: a review, Eur. Polym. J. 136 (2020), 109912, https://doi.org/10.1016/j.eurpolymj.2020.109912.

[3] S. Basak, A. Bandyopadhyay, Solvent responsive shape memory polymers-Evolution, current status, and future outlook, Macromol. Chem. Phys. 222 (19) (2021), 2100195, https://doi.org/10.1002/macp.202100195.

[4] Q.J. Ze, X. Kuang, S. Wu, J. Wong, S.M. Montgomery, R.D. Zhang, J.M. Kovitz, F. Y. Yang, H.J. Qi, R.K. Zhao, Magnetic shape memory polymers with integrated multifunctional shape manipulation, Adv. Mater. 32 (4) (2020), 1906657, https://doi.org/10.1002/adma.201906657.

[5] W.B. Li, J.H. Liu, L. Chen, W.T. Wei, K. Qian, Y.J. Liu, J.S. Leng, Application and development of shape memory micro/nano patterns, Small 18 (13) (2022), 2105958, https://doi.org/10.1002/smll.202105958.

[6] S. Yang, Y. He, Y.J. Liu, J.S. Leng, Non-contact magnetic actuated shape-programmable poly(aryl ether ketone)s and their structural variation during the deformation process, Smart Mater. Struct. 31 (3) (2022), 035035, https://doi.org/10.1088/1361-665X/ac4ff7.

[7] S. Pringpromsuk, H. Xia, Q.Q. Ni, Multifunctional stimuli-responsive shape memory polyurethane gels for soft actuators, Sensor Actuat. A-Phys. 313 (2020), 112207, https://doi.org/10.1016/j.sna.2020.112207.

[8] W. Luo, J.X. Liu, C.H. Fang, B.P. Liu, H.T. Xia, H.J. Li, J. Huang, Templating assembly of NIR light-actuated TPU/SCNT-C-60 flexible structures with high conductivity and controllable recovery behavior, Surface. Interfac. 25 (2021), 1011230, https://doi.org/10.1016/j.surfin.2021.101230.

[9] H.R. Chen, H. Xia, Y.P. Qiu, Z.Z. Xu, Q.Q. Ni, Smart composites of piezoelectric particles and shape memory polymers for actuation and nanopositioning, Compos. Sci. Technol. 163 (2018) 123–132, https://doi.org/10.1016/j.compscitech.2018.05.004.

[10] X.F. Jiang, B.K. Tian, X.Y. Xuan, W.Q. Zhou, J.X. Zhou, Y.Q. Chen, Y. Lu, Z. H. Zhang, Cellulose membranes as moisture-driven actuators with predetermined deformations and high load uptake, Int. J. Smart Nano Mat. 12 (2) (2021) 146–156, https://doi.org/10.1080/19475411.2021.1906780.

[11] B.J. Jin, H.J. Song, R.Q. Jiang, J.Z. Song, Q. Zhan, T. Xie, Programming a crystalline shape memory polymer network with thermo- and photo-reversible bonds toward a single-component soft robot, Sci. Adv. 4 (1) (2018) eaao3865, https://doi.org/10.1126/sciadv.aao3865.

[12] H. Gao, J.R. Li, F.H. Zhang, Y.J. Liu, J.S. Leng, The research status and challenges of shape memory polymer-based flexible electronics, Mater. Horiz. 6 (5) (2019) 931–944, https://doi.org/10.1039/C8MH01070F.

[13] J.M. Korde, B. Kandasubramanian, Naturally biomimicked smart shape memory hydrogels for biomedical functions, Chem. Eng. J. 379 (2020), 122430, https://doi.org/10.1016/j.cej.2019.122430.

[14] J.H. Jang, S.B. Hong, J.G. Kim, N.S. Goo, H. Lee, W.R. Yu, Long-term properties of carbon fiber-reinforced shape memory epoxy/polymer composites exposed to

vacuum and ultraviolet radiation, Smart Mater. Struct. 28 (11) (2019), 115013, https://doi.org/10.1088/1361-665X/ab3fda.
[15] H.T. Lv, D.Y. Tang, Z.J. Sun, J.R. Gao, X. Yang, S.Y. Jia, J. Peng, Electrospun PCL-based polyurethane/HA microfibers as drug carrier of dexamethasone with enhanced biodegradability and shape memory performances, Colloid Polym. Sci. 298 (1) (2020) 103–111, https://doi.org/10.1007/s00396-019-04568-5.
[16] Y.T. Yao, Y. Luo, H.B. Lu, B. Wang, Remotely actuated porous composite membrane with shape memory property, Compos. Struct. 192 (2018) 507–515, https://doi.org/10.1016/j.compstruct.2018.03.060.
[17] C.H. Hsieh, N.A.M. Razali, W.C. Lin, Z.W. Yu, D. Istiqomah, Y. Kotsuchibashi, H. H. Su, Development of thermo-responsive polycaprolactone–polydimethylsiloxane shrinkable nanofibre mesh, Nanomaterials 10 (7) (2020) 1427, https://doi.org/10.3390/nano10071427.
[18] A. Sonseca, S. Madani, A. Muoz-Bonilla, M. Fernandez-Garcia, L. Peponi, A. Leones, G. Rodriguez, C. Echeverria, D. Lopez, Biodegradable and antimicrobial PLA–OLA blends containing chitosan-mediated silver nanoparticles with shape memory properties for potential medical applications, Nanomaterials 10 (6) (2020) 1065, https://doi.org/10.3390/nano10061065.
[19] S.Q. Ma, S.L. Wang, S.Z. Jin, Y.Q. Wang, J.N. Yao, X.G. Zhao, C.H. Chen, Construction of high-performance, high-temperature shape memory polyimides bearing pyridine and trifluoromethyl group, Polymer 210 (5) (2020), 122972, https://doi.org/10.1016/j.polymer.2020.122972.
[20] W. Jian, X.D. Wang, H.B. Lu, D. Lau, Molecular dynamics simulations of thermodynamics and shape memory effect in CNT-epoxy nanocomposites, Compos. Sci. Technol. 211 (2021), 108849, https://doi.org/10.1016/j.compscitech.2021.108849.
[21] Z.H. Li, J.K. Hu, L. Ma, H.X. Liu, High glass transition temperature shape-memory materials: hydroxyl-terminated polydimethylsiloxane-modified cyanate ester, J. Appl. Polym. Sci. 137 (18) (2019), 48641, https://doi.org/10.1002/app.48641.
[22] B.H. Chen, L. Yuan, Q.B. Guan, G.Z. Liang, A.J. Gu, Preparation and mechanism of shape memory bismaleimide resins with high transition temperature, high toughness and good processability, J. Mater. Sci. 53 (15) (2018) 10798–10811, https://doi.org/10.1007/s10853-018-2367-4.
[23] K. Ren, Q.Q. Xia, Y.Z. Liu, W.K. Cheng, Y. Liu, H.P. Yu, Wood/polyimide composite via a rapid substitution compositing method for extreme temperature conditions, Compos. Sci. Technol. 207 (2021), 108698, https://doi.org/10.1016/j.compscitech.2021.108698.
[24] J. Yao, S. Ma, J. Zhang, Y. Wang, C. Wang, H. Zhou, C. Chen, G. Liu, Multiple shape memory effects of polyimide nanocomposites based on octa(aminophenyl) silsequioxanes, Express Polym. Lett. 15 (5) (2021) 433–444, https://doi.org/10.3144/expresspolymlett.2021.37.
[25] Z.X. Lan, X.L. Chen, X. Zhang, C.Y. Zhu, Y.L. Yu, J. Wei, Transparent, high glass-transition temperature, shape memory hybrid polyimides based on polyhedral oligomeric silsesquioxane, Polymers 11 (6) (2019) 1058, https://doi.org/10.3390/polym11061058.
[26] X.F. Wang, Y. He, J.S. Leng, Shape memory polyimides and composites with tunable chain stiffness and ultrahigh transition temperature range, Composer Part A: Appl. S. 163 (2022), 107237, https://doi.org/10.1016/j.compositesa.2022.107237.
[27] K. Kim, J. Kim, Fabrication of thermally conductive composite with surface modified boron nitride by epoxy wetting method, Ceram. Int. 40 (4) (2014) 5181–5189, https://doi.org/10.1016/j.ceramint.2013.10.076.
[28] S. Nagaoka, T. Jodai, Y. Kameyama, Cellulose/boron nitride core–shell microbeads providing high thermal conductivity for thermally conductive composite sheets, RSC Adv. 6 (39) (2016) 33036–33042, https://doi.org/10.1039/c6ra02950g.
[29] X.L. Ao, D.Y. Kong, Z.Y. Zhang, X.L. Xiao, Enhancing recovery speed and anti-wear capability of high-temperature shape memory polymer with modified boron nitride nanoparticles, J. Mater. Sci. 55 (10) (2020) 4292–4302, https://doi.org/10.1007/s10853-019-04319-5.
[30] D.W. Zhang, F.S. Liu, S. Wang, M.X. Yan, X. Hu, M.Y. Xu, D-GQDs modified epoxy resin enhances the thermal conductivity of AlN/epoxy resin thermally conductive composites, Polymers 13 (23) (2021) 4074, https://doi.org/10.3390/polym13234074.
[31] W.Y. Peng, X.Y. Huang, J.H. Yu, P.K. Jiang, W.H. Liu, Electrical and thermophysical properties of epoxy/aluminum nitride nanocomposites: effects of nanoparticle surface modification, Composer Part A: Appl. S. 41 (9) (2010) 1201–1209, https://doi.org/10.1016/j.compositesa.2010.05.002.
[32] Y. Zhou, J. Hu, X. Chen, F. Yu, J.L. He, Thermoplastic polypropylene/aluminum nitride nanocomposites with enhanced thermal conductivity and low dielectric loss, IEEE Trans. Dielectr. Electr. Insul. 23 (5) (2016) 2768–2776, https://doi.org/10.1109/TDEI.2016.005994.
[33] Y.C. Wu, F.L. Lin, X.T. Lin, Y.J. Liu, L.J. Song, X.H. Hao, J.L. Li, S.L. Wang, The synergistic effect of irregular alumina and round plates boron nitride binary-particle system on the thermal conductivity of epoxy composites, J. Appl. Polym. Sci. 139 (8) (2022), e51658, https://doi.org/10.1002/app.51658.
[34] Z. Barani, A. Mohammadzadeh, A. Geremew, C.Y. Huang, D. Coleman, L. Mangolini, F. Kargar, A.A. Balandia, Thermal properties of the binary-filler hybrid composites with graphene and copper nanoparticles, Adv. Funct. Mater. 30 (8) (2020), 1904008, https://doi.org/10.1002/adfm.201904008.
[35] X.H. He, Y.C. Wang, Highly thermally conductive polyimide composite films with excellent thermal and electrical insulating properties, Ind. Eng. Chem. Res. 59 (5) (2020) 1925–1933, https://doi.org/10.1021/acs.iecr.9b05939.
[36] D.I. Arun, P. Chakravarthy, K.S. Santhosh, Synergy studies on polyurethane-carbon black, multi-walled carbon nanotube-based heterogeneous electroactive shape memory nanocomposite system, Bull. Mater. Sci. 43 (1) (2020) 219, https://doi.org/10.1007/s12034-020-02213-4.
[37] Y. Wang, X.S. Qiao, J. Wan, Y. Xiao, X.P. Fan, Preparation of AlN microspheres/UHMWPE composites for insulating thermal conductors, RSC Adv. 6 (83) (2016) 80262–80267, https://doi.org/10.1039/c6ra18228c.
[38] X.L. Zeng, J.J. Sun, Y.M. Yao, R. Sun, J.B. Xu, C.P. Wong, A combination of boron nitride nanotubes and cellulose nanofibers for the preparation of a nanocomposite with high thermal conductivity, ACS Nano 11 (5) (2017) 5167–5178, https://doi.org/10.1021/acsnano.7b02359.
[39] X.Z. Huang, F.H. Zhang, Y.J. Liu, J.S. Leng, Flexible and colorless shape memory polyimide films with high visible light transmittance and high transition temperature, Smart Mater. Struct. 28 (5) (2019), 055031, https://doi.org/10.1088/1361-665X/ab115f.
[40] Q.H. Wang, Y.K. Bai, Y. Chen, J.P. Ju, F. Zeng, T.M. Wang, High performance shape memory polyimides based on π-π interactions, J. Mater. Chem. 3 (1) (2015) 352–359, https://doi.org/10.1039/C4TA05058D.
[41] Z.H. Yang, Q.H. Wang, T.M. Wang, Tunable triple-shape memory binary mixtures with high transition temperature and robust mechanical properties, Macromol. Chem. Phys. 217 (11) (2016) 1305–1313, https://doi.org/10.1002/macp.201500539.
[42] X.F. Li, L.C. Wang, Z.Y. Zhang, D.Y. Kong, X.L. Ao, X.L. Xiao, Electroactive high-temperature shape memory polymers with high recovery stress induced by ground carbon fibers, Macromol. Chem. Phys. 220 (17) (2019), 1900164, https://doi.org/10.1002/macp.201900164.
[43] Z.H. Yang, F.Z. Song, Q.H. Wang, T.M. Wang, Shape memory induced structural evolution of high performance copolyimides, J. Polym. Sci. Part A 54 (24) (2016) 3858–3867, https://doi.org/10.1002/pola.28356.
[44] S. Choi, J. Kim, Thermal conductivity of epoxy composites with a binary-particle system of aluminum oxide and aluminum nitride fillers, Compos. B Eng. 51 (2013) 140–147, https://doi.org/10.1016/j.compositesb.2013.03.002.
[45] J.J. Sun, Y.M. Yao, C.P. Wong, Preparation of boron nitride nanosheet/nanofibrillated cellulose nanocomposites with ultrahigh thermal conductivity via engineering interfacial thermal resistance, Adv. Mater. Interfac. 4 (17) (2017), 1700563, https://doi.org/10.1002/admi.201700563.